Development of numerical model for buoyancy-driven heat transfer between parallel plates

Mateo Kirinčić[1,*], Tin Fadiga[1], Fran Torbarina[2], Paolo Blecich[1]
University of Rijeka, Faculty of Engineering, Vukovarska 58, Rijeka. Croatia[1]
University of Rijeka, Faculty of Maritime Studies, Studentska 2, Rijeka, Croatia[2]
mateo.kirincic@riteh.uniri.hr

Abstract: *The main objective of this study is to develop and experimentally validate a finite volume numerical model for buoyancy-driven (natural convective) heat transfer between parallel plates representative of plate fin passive heat sinks. The validation employs a calorimetry-based setup: a vertical aluminum plate fin heat sink is mounted to the only uninsulated wall of an otherwise well-insulated, water-filled rectangular vessel that serves as a controllable heat source. The total heat transfer rate and convective heat transfer coefficients are inferred from the time evolution of the calorimetric water temperature, and fin surface temperatures are measured at several characteristic locations. The model resolves conjugate heat transfer between the solid heat sink and the surrounding air. Numerical predictions of heat transfer rate, fin surface temperatures, and convective heat transfer coefficients show good agreement with measurements and with established literature correlations, confirming the validity of the mathematical model and numerical procedure. The developed numerical model can be used for further analyses and optimization processes.*

Keywords*: PARALLEL PLATES, BUOYANCY-DRIVEN HEAT TRANSFER, NUMERICAL MODEL, FINITE VOLUME METHOD, EXPERIMENTAL VALIDATION.*

1. Introduction

Driven by Moore's law, successive doublings of transistor density, device power densities and attendant heat loads have escalated. Computational capability has outpaced our ability to remove waste heat without throttling, making thermal management a primary constraint. In high-power electronics, lighting, and renewable-energy converters, it affects not only efficiency but also reliability, service life, and safety [1].

A heat sink rejects heat from a solid surface to the surrounding fluid (typically air) through conduction within the solid, convection at the surface, and radiation to the environment; the radiative share depends on surface emissivity. By cooling mode, heat sinks are passive, active, or hybrid. Active designs employ forced convection, usually fans or blowers, to boost heat transfer and are common in dense electronics such as CPUs and telecom hardware [2]. Passive designs rely on natural convection and radiation, suiting applications that prioritize silence, low maintenance, and high reliability, e.g. LED lights, PV inverters, and aerospace systems [3].

Plate fin heat sinks are prevalent due to predictable performance and straightforward fabrication, whereas pin fin arrays [4] can provide more isotropic cooling under multidirectional flows. To intensify convection by disturbing boundary layers, many geometries have been investigated: rippled fins [5], dimpled fins [6], louvered fins [7], perforated fins [8], etc. Orientation matters as well: vertical mounting promotes stable buoyant plumes, while horizontal or inclined placement typically diminish heat transfer [9].

Foundational analyses of natural convection in vertical fin arrays trace back to Elenbaas [10]. The framework of Bar-Cohen and Rohsenow [11] remains central, offering semi-analytical guidance for thermally optimal fin spacing by balancing conductive and convective resistances. Beyond such analytical and semi-analytical work, passive heat sinks have been extensively studied through experiments and numerical simulations.

Mehrtash and Tari [12] used a validated numerical model to study natural convection from inclined plate-fin heat sinks. By rotating the gravity vector, they examined inclinations from −60° to 90° over a wide Rayleigh number range (up to about 2×10^8) and proposed a generalized correlation to predict convective heat transfer for rectangular plate-fin arrays at different angles. Using a validated pin-fin correlation together with established plate-fin relations, Joo and Kim [13] optimized both heat sink types for a fixed base-to-ambient temperature difference and identical base size and fin height. Two objectives were considered: total heat removed and heat removed per unit mass. Plate fins outperformed in total heat removal, while pin fins excelled on a per-mass basis, enabling lighter designs with higher specific performance. Ahmadi et al. [14] performed a combined numerical–experimental investigation of steady natural convection from vertically mounted rectangular interrupted fins. A two-dimensional model and a custom rig with 12 aluminum heat sinks supported a parametric study of fin spacing and interruption length; interruptions markedly improved performance and exhibited an optimal length. Quintino et al. [15] numerically mapped natural convection between two vertical plates, varying Rayleigh number, nondimensional horizontal spacing, and vertical alignment. They identified an alignment and Rayleigh-dependent optimal spacing that maximizes total Nusselt number: the optimum decreases as Rayleigh number increases and as the plates approach a face-to-face configuration. For large gaps the plates behave independently; at intermediate gaps, reduced stagger strengthens the chimney effect; and for very tight gaps, greater stagger improves exposure. Fuse et al. [16] varied both base and ambient temperatures in their measurements, supplying useful datasets for CFD validation and showing that shifts in ambient temperature can materially alter the optimal design point.

Building on prior studies, this work develops a finite volume numerical model that treats density using the incompressible ideal gas formulation. The model is validated experimentally through a series of calorimetric tests. The validated model is suitable for further numerical analyses, and the accompanying measurements broaden the experimental record and can serve as reference data for validating other numerical models**.**

2. Physical problem and mathematical model

An extruded aluminum heat sink with straight vertical plate fins (shown in Fig**.** 1) was selected from commercial stock. No surface treatment was applied; the surfaces are bare aluminum. The heat sink measures 123 mm in width (W) and 100 mm in length (L). The base is 6 mm thick (δ_b) and carries 11 identical fins. Each fin is rectangular, 3 mm thick (δ_f), 30 mm in height (H), and extends the full 100 mm length (L), with a spacing (s) of 9 mm between fins. The base area is 0.0123 m^2, and the area exposed to air is 0.082 m^2. This geometry was used in the subsequent experiments and simulations.

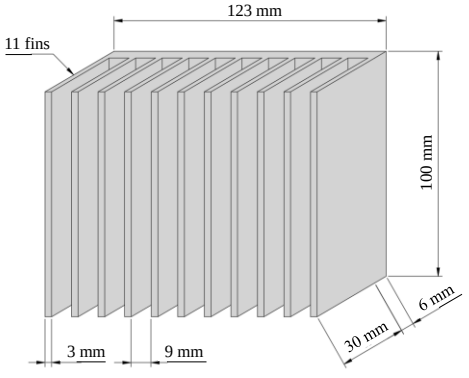

Fig. 1 *Analyzed passive heat sink.*

In passive cooling devices, heat produced by the component is conducted into the base, spreads laterally and through the fin array, and is carried along each fin from base to tip, establishing a temperature gradient. At the fin surfaces, heat is transferred to the surrounding air by natural convection as the warmed air adjacent to the fins rises and is replaced by cooler ambient air. As shown in Fig. 1, the heat-sink geometry is symmetric in length and height; however, because natural convection develops in the vertical direction, physical symmetry applies only across the width. Consequently, modeling one half of the width is sufficient for the numerical analysis and captures all relevant processes, substantially reducing computational effort while maintaining accuracy.

To describe the flow around the heat sink, a surrounding air enclosure was defined. In the vertical direction it extends 100 mm below the bottom of the heat sink and 100 mm above its top. In the lateral direction it extends 30 mm beyond the side. In the front-to-back direction it reaches 90 mm outward from the fin tips in front and 30 mm from the base behind. The region directly behind the base is not included because that surface is in contact with the electronic component. The resulting computational domain consists of two subdomains: the aluminum heat sink and the surrounding air, and is shown in Figure 2.

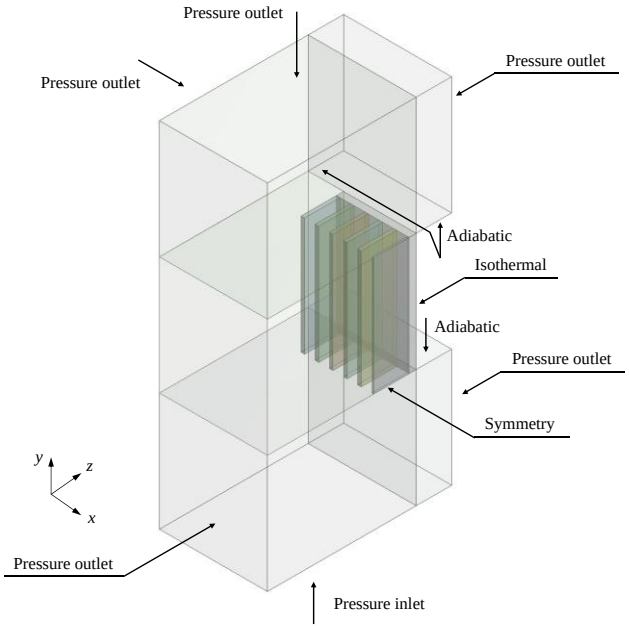

Fig. 2 *Computational domain and boundary conditions.*

The problem is treated as steady-state conjugate heat transfer: heat conducts within the heat sink while natural convection develops in the surrounding air. A three-dimensional model was formulated with the following assumptions. The solid heat sink is homogeneous and isotropic, and its thermophysical properties are taken as constant. The airflow is steady and laminar, driven solely by buoyancy; density variations are introduced via the incompressible ideal gas relation, while all other fluid properties are held constant and evaluated at the film temperature. Viscous dissipation and thermal radiation are neglected. The mid-width symmetry plane is modeled as adiabatic and impermeable, the heat sink base is assigned a uniform temperature, and the ambient air temperature far from the sink is prescribed as constant. Thermophysical properties of air are as follows: thermal expansion coefficient, 0.0032 1/K; density, 1.13 kg/m^3; thermal conductivity, 0.0267 W/m□ K; specific heat capacity, 1007 J/kg□ K; dynamic viscosity, 1.872□ 10^5 Pa□ s.

For the present problem, the conservation equations for mass and momentum are applied in the fluid (air) subdomain, whereas the energy conservation equation is applied in both the solid (aluminum) and fluid subdomains. Boundary conditions were specified on the domain's outer faces and at the solid–fluid interface between the heat sink and the surrounding air (as seen in Fig. 2).

3. Numerical setup and procedure

The problem was solved with the finite volume method [17] using ANSYS Fluent. Pressure–velocity coupling was handled with the SIMPLE algorithm, with density treated as a function of temperature only, not influenced by local pressure fluctuations. Pressure was discretized with the PRESTO! scheme, and convective terms in the momentum and energy equations were discretized with a second-order upwind scheme. To improve numerical stability in the incompressible ideal-gas formulation, an operating density corresponding to the ambient temperature was specified to stabilize the pressure field. Under-relaxation factors of 0.3, 0.6, and 1 were used for pressure, momentum, and energy, respectively. Convergence was deemed achieved when residuals fell below 10^{-3} for continuity and 10^{-6} for momentum and energy.

Mesh independence was assessed by comparing the specific heat flux at the heat sink surface for three meshes, with 525900, 4119600 and 8968725 cells. Differences were small across all cases, with the smallest relative change between the two finest meshes, indicating mesh-independent results. The mesh with 4119600 cells was therefore adopted for all subsequent simulations.

4. Experimental validation

To evaluate the validity of the mathematical model and numerical procedure, numerical heat transfer rates and heat transfer coefficients were compared with measurements obtained using a custom-built experimental apparatus. For experimental validation, a test heat sink was examined in the laboratory through a series of calorimetric runs. Because the numerical treatment includes only natural convection, a polished aluminum heat sink was used to minimize radiation. It has been observed [18] that for low-emissivity heat sinks, radiation contributes about 5% or less of the total heat transfer, which is negligible for the present purposes.

To emulate the thermal load of an electronic component, a tin vessel filled with a known mass of water served as the heat source (Fig. 3). The heat sink was rigidly mounted to one side of the vessel, with a thin, uniform layer of silicone thermal paste applied at the interface to reduce contact resistance [19]. To limit environmental losses, all vessel faces except the contact surface were insulated with expanded rubber foam and covered with aluminum foil to reduce radiative exchange.

The experiment commenced once water at a uniform initial temperature was poured into the vessel. After the initial unsteady stage, characterized by significant temperature variations, the system entered a quasi-steady regime in which the water temperature fell approximately linearly and heat sink surface temperatures showed only small variations. Temperatures were recorded continuously at 1-s intervals. The bulk water and ambient air temperatures were measured with thermistor probes (accuracy ±0.02 °C). To capture the transient response at characteristic locations on the heat sink surfaces, four K-type thermocouples (s1–s4, accuracy ±0.2 °C) were placed along the width and height of a representative inner fin (also shown in Fig. 3), and one thermocouple was placed between the heat sink base and the vessel.

Three experiments were conducted, each starting from a different initial water temperature. In all cases, the water mass was 3.467 kg (scale accuracy ±0.005 kg), the specific heat of water was taken as 4184 J/kg·K, and the quasi-steady period lasted 16 minutes. After the initial unsteady stage, the bulk water temperature decreased approximately linearly, while the four surface thermocouples remained within a narrow band throughout the quasi-steady interval. The ambient temperature was essentially constant over the entire test.

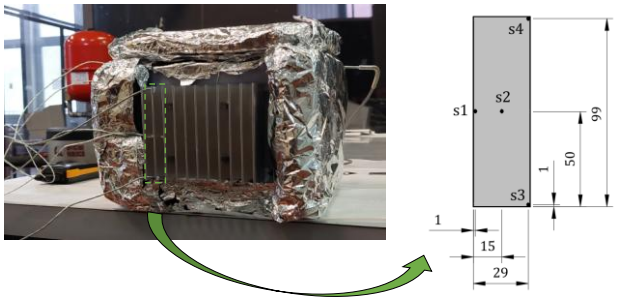

Fig. 3 *Experimental apparatus and heat sink surface temperatures sensors positions.*

Heat sink base and surface temperatures were averaged over the quasi-steady window of 16 min. The change in bulk water temperature between the start and end of this window was then used to determine the average heat transfer rate and the heat transfer coefficient. Table 4 reports averaged temperatures on the base surface (T_b), mean fin surface temperature (T_s), and in the surrounding air (T_a) for all three runs. The table also includes the water bulk temperature change ΔT_w, and the derived values of heat transfer rate $\left(\dot{Q}\right)$ and heat transfer coefficient (h).

Table 1. *Experimentally obtained temperatures at heat sink base and surface, air, bulk water temperature change, and derived heat transfer rates and heat transfer coefficient for all three runs.*

Obtained quantity	Run 1	Run 2	Run 3
T_b [°C]	42.3	50	59.8
T_s [°C]	42.05	49.63	59.28
T_a [°C]	28.39	29.02	28.61
ΔT_w [°C]	0.38	0.61	0.96
$\dot{Q}$ [W]	5.74	9.47	14.51
h [W/m^2□ K]	5.13	5.46	5.77

The operating conditions used in the simulations, i.e. ambient temperature and heat sink base temperature, matched those in the experiments. Fig. 4 compares the heat transfer rates and heat transfer coefficients obtained numerically and experimentally across the tested base temperatures.

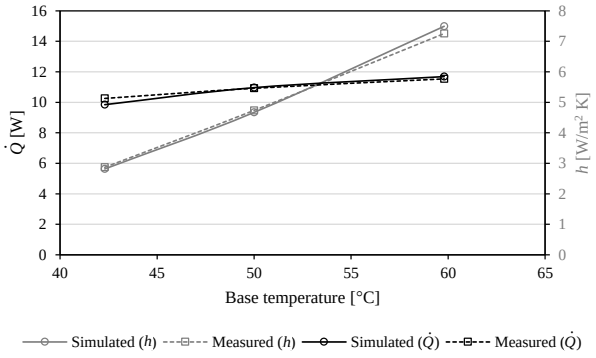

Fig. 4 *Comparison of simulated and measured heat transfer rates and heat transfer coefficients across investigated base temperatures.*

Fig. 4 indicates close agreement between the simulated and measured heat transfer rates and heat transfer coefficients across the examined base temperature range. For base temperatures of 42.3, 50, and 59.8 °C, the simulated values of heat transfer rates are 5.64, 9.22, and 14.99 W, all corresponding well with their experimentally obtained equivalents. Similarly, for investigated base temperatures, the simulations predict heat transfer coefficients of 4.93, 5.48, and 5.84 W/m^2□K, all in good agreement with those derived from measurements. Overall, the consistency across methods supports that the model and numerical setup capture the heat sink heat transfer behavior and are suitable for further numerical analyses.

For the conditions in run 2, temperature profiles along the fin height and along the fin length were also compared between numerical and experimental results. Experimental profiles were taken at the predefined thermocouple locations: 1 and 2 at mid-fin length along the height, and 3 and 4 near the fin tip along the length. Fig. 5 presents the comparison between simulated and measured temperature profiles.

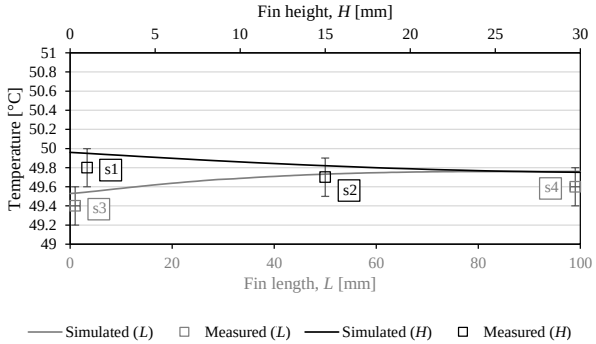

Fig. 5 *Comparison of simulated and measured temperature profiles along the fin height and length for base temperature 50 °C and air temperature 29 °C (run 2).*

As seen from Fig. 5, simulated and measured profiles along the fin height and length show good agreement. In the height direction, temperature decreases with increasing distance from the base, reflecting conductive heat flow from the hotter base toward the fin tip. In the lengthwise direction, temperatures rise gradually: the air is coolest near the bottom, leading to stronger local convection and lower surface temperatures there; farther along the passage between fins the air warms, the temperature difference is reduced, and slightly higher surface temperatures result. These trends are consistent with the physical process of natural convection and further support the consistency between the experimental and numerical results.

5. Numerical results

In order to characterize the heat dissipation through the heat sink, temperature distributions at characteristic domain segments, obtained for the case with the base temperature of 50 °C and ambient temperature of 29 °C, i.e. run 2, have been presented. Fig. 6 shows the temperature distribution in the vertical plane for H = 15 mm, i.e. the fin mid-height section.

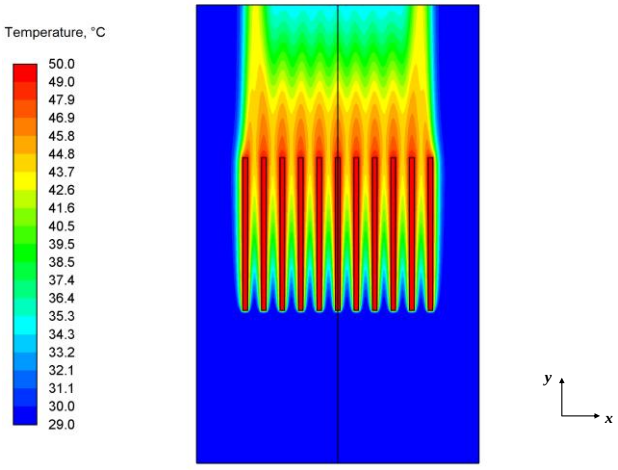

Fig. 6 *Temperature distribution at the fin mid-height section for base temperature 50 °C and air temperature 29 °C (run 2).*

Fig. 6 shows the uniformity in temperature distribution throughout all slots, i.e. flow passages between the fins. In each slot between the fins, boundary layers are uniformly formed from the bottom in the airflow direction. Air particles near the fins get warmer, thus lighter, and are driven upward due to buoyancy. The air temperature in each slot is the highest at the edges of each flow passage, i.e. near the fins, and decreases toward the center of each flow passage, which is consistent with boundary layer development. Each slot promotes the formation of its own thermal plume, which all span above the heat sink, demonstrating an effective natural convection-governed heat dissipation.

As can be seen from both experimental and numerical results, temperatures within the heat sink span a very small range. In order to better perceive the heat dissipation from the base to the surface, the local temperature distribution for the heat sink is given in Fig. 7.

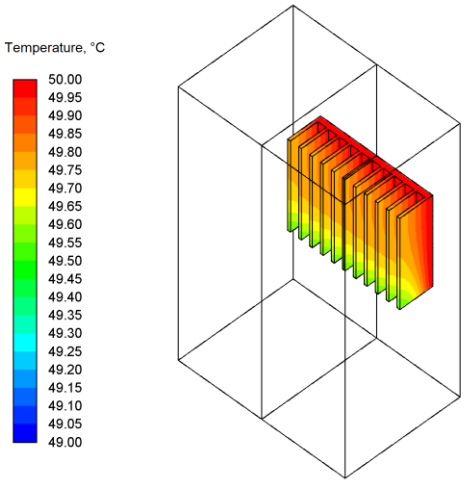

Fig. 7 *Local heat sink temperature distribution for base temperature 50 °C and air temperature 29 °C (run 2).*

Fig. 7 shows that the heat sink surface temperature distribution is fairly uniform for all fins, with outer fins being just slightly cooler than the inner due to their greater exposure to the surrounding air. It can also be observed that the heat sink base, held at constant temperature, is the hottest region. Temperature then decreases progressively along the fin height as heat is conducted through the solid and dissipated to the surrounding air by natural convection. The temperature profile on the fins' surfaces reflects nonuniform heat transfer. At the bottom, the incoming air is cooler, so the thermal gradient between the fin surface and the surrounding air is larger, resulting in stronger convective heat removal. As the air warms while rising through the slots between the fins, the local temperature difference decreases, so convective heat transfer weakens at the top of the fins.

6. Conclusion

In the paper, a numerical model describing buoyancy-driven heat transfer between parallel plates was developed. Its accuracy was established through a robust validation protocol that compared simulated and measured heat transfer rates, heat transfer coefficients, and fin temperature profiles from calorimetric experiments. Agreement across all metrics and operating conditions supports the model fidelity to the underlying physics. The validated framework is suitable for further numerical studies, with accompanying measurements providing reference for future model verification.

Acknowledgement: This work has been supported by the University of Rijeka under the project number "uniri-mladi-tehnic-23-8".

7. References

1. H.B. Ghadim, M.M. Davodi, F. Rezaei, A. Jafari, M. Eslami, "Review of thermal management of electronics and phase change materials," Renewable and Sustainable Energy Reviews 208, 115039 (2025).
2. E. Öztürk, I. Tari, "Forced air cooling of CPUs with heat sinks: A numerical study," IEEE Transactions on Components and Packaging Technologies 31(3), 650–660 (2008).
3. H.A. Kazem, A.H.A. Al-Waeli, M.T. Chaichan, K. Sopian, A. Al-Amery, W.I. Wan Nor Roslam, "Enhancement of photovoltaic module performance using passive cooling (fins): A comprehensive review," Case Studies in Thermal Engineering 49, 103316 (2023).
4. M. Ismail, "Experimental and numerical analysis of heat sink using various patterns of cylindrical pin-fins," International Journal of Thermofluids 23, 100737 (2024).
5. I. El Ghandouri, A. El Maakoul, S. Saadeddine, M. Meziane, "Design and numerical investigations of natural convection heat transfer of a new rippling fin shape," Applied Thermal Engineering 178, 115670 (2020).
6. S.-W. Chang, H.-W. Wu, D.-Y. Guo, J.-J. Shi, T.-H. Chen, "Heat transfer enhancement of vertical dimpled fin array in natural convection," International Journal of Heat and Mass Transfer 106, 781–792 (2017).
7. A.C. Lyman, R.A. Stephan, K.A. Thole, L.W. Zhang, S.B. Memory, "Scaling of heat transfer coefficients along louvered fins," Experimental Thermal and Fluid Science 26(5), (2002).
8. U.V. Awasarmol, A.T. Pise, "An experimental investigation of natural convection heat transfer enhancement from perforated rectangular fin arrays at different inclinations," Experimental Thermal and Fluid Science 68, 145–154 (2015).
9. X. Huang, C. Shi, J. Zhou, L. Zhang, Z. Xu, "Performance analysis and design optimization of heat pipe sink with a variable height fin array under natural convection," Applied Thermal Engineering 160, 113939 (2019).
10. W. Elenbaas, "The dissipation of heat by free convection from vertical and horizontal cylinders," Journal of Applied Physics 19(12), 1148–1154 (1948).
11. A. Bar-Cohen, W.M. Rohsenow, "Thermally optimum spacing of vertical, natural convection-cooled, parallel plates," Journal of Heat Transfer 106(1), 116–123 (1984).
12. M. Mehrtash, I. Tari, "A correlation for natural convection heat transfer from inclined plate-finned heat sinks," Applied Thermal Engineering 51, 1067–1075 (2013).
13. Y. Joo, S.J. Kim, "Comparison of thermal performance between plate-fin and pin-fin heat sinks in natural convection," International Journal of Heat and Mass Transfer 83, 345–356 (2015).
14. M. Ahmadi, G. Mostafavi, M. Bahrami, "Natural convection from rectangular interrupted fins," International Journal of Thermal Sciences 82, 62–71 (2014).
15. A. Quintino, M. Cianfrini, I. Petracci, V.A. Spena, M. Corcione, "Dimensionless correlations for natural convection heat transfer from a pair of vertical staggered plates suspended in free air," Applied Sciences 11, 6511 (2021).
16. H. Fuse, S. Oe, T. Haga, "Effects of fin height, base thickness, blackening, emissivity and thermal conductivity on heat dissipation of die-cast aluminum alloy heat sink," Metals 15, 696 (2025).
17. H.K. Versteeg, W. Malalasekera, An Introduction to Computational Fluid Dynamics: The Finite Volume Method, 2nd ed. (Pearson, 2007).
18. T. Aihara, S. Maruyama, S. Kobayakawa, "Free convective/radiative heat transfer from pin-fin arrays with a vertical base plate (general representation of heat transfer performance)," International Journal of Heat and Mass Transfer 33(6), 1223–1232 (1990).
19. T. Fadiga, Investigation of heat transfer through a heat sink, Master's thesis (University of Rijeka, Faculty of Engineering, Rijeka, Croatia, 2025) [in Croatian].